ACS OMEGA

Open Access

http://pubs.acs.org/journal/acsodf

Article

Solvothermal Preparation of Crystal Seeds and Anisotropy-Controlled Growth of Silver Nanoplates

Zhenbin Zhang, Tanlong Xue, Mingli Qin, Yanzhao Wang, Qi Shi, Lulu Wang, Yanhong Zhao,* and Zhimin Yang*

Cite This: *ACS Omega* 2024, 9, 28659−28665

Read Online

ACCESS | Metrics & More | Article Recommendations | Supporting Information

ABSTRACT: We synthesized silver nanoplates using the solvothermal method and, for the first time, placed them as crystal seeds in a water-based growth solution, thereby successfully achieving the large-scale production of silver nanoplates. The synthesis method enabled independent control of the lateral size and vertical size of the silver nanoplates. More specifically, the lateral size could be adjusted within the range of 565 nm−1.682 μm, while the vertical size was achieved by introducing Cl^- as a capping agent and the vertical size was thickened from 18.28 to 40.41 nm.

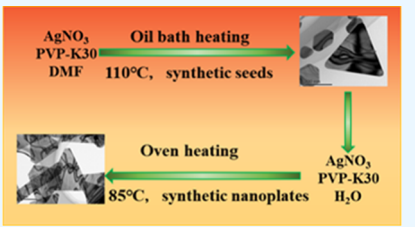

1. INTRODUCTION

Silver (Ag) nanoparticles have attracted extensive interest due to their excellent conductivity, tunable optical properties, and sintering properties.[1−3] In general, those physical and chemical properties were affected dramatically by the size and shape of nanoparticles. Thus, the synthesis of silver nanoparticles with a specific shape is of great importance. Silver nanoplates (also known as nanoprisms and nanodisks) belong to two-dimensional nanostructures. Compared to other shapes of silver nanoparticles, silver nanoplates possessed high anisotropy that favors highly tunable local surface plasmon resonances and enhanced local electromagnetic field.[4] At the same time, the vertical size of as-prepared nanoplates can be controlled at the level of several nanometers, and its sharp corner has high free energy, so that it has a large driving force for sintering. Therefore, its sintering temperature can be much lower than the melting point of bulk silver, which might be used for flexible circuit printing, biosensors, micronano chip packaging, etc.[5−8]

Since Mirkin and coworkers reported the conversion of silver nanospheres into triangular nanoplates by fluorescent lamps in 2001, a large number of synthetic routes have emerged, including light- or heat-induced conversion and direct chemical reduction.[9] At present, most of the relevant literature on silver nanoplates can achieve controllable preparation of triangular silver nanoplates in a low concentration of silver source or organic system (this is shown in Table S1) which inevitably causes low yield and environmental pollution. To increase the concentration of Ag^+ in the preparation process, the crystal seed growth method is often used. However, in the reported synthesis methods for silver nanoplates based on crystal seed growth, the crystal seeds were usually prepared in the aqueous system and then placed in the aqueous system for growth. Besides, toxic substances such as acetonitrile were used to inhibit spontaneous nucleation. Although the concentration of Ag^+ in the preparation process was improved, the improvement is not obvious enough. The preparation process usually requires extremely high centrifugation speed to collect crystal seeds, which is not convenient for most laboratories.[10−12] Thus, the current preparation method is unsuitable for the large-scale industrial application of silver nanoplates.

The quality of the crystal seeds is crucial in the seed-mediated synthesis of the silver nanoplates. In order to ensure the quality of the subsequent growth, the crystal seeds cannot contain silver nanoparticles of other shapes (sphere-like or wire-like). However, due to the large specific surface area of silver nanoplates and the lattice strain energy caused by defects, the total free energy of silver nanoplates is too high to exist in solution.[13,14] Therefore, kinetic control is required to change the reduction or decomposition rate of the precursor in order to control the population of the seeds with twin defects. When the decomposition or reduction rate of the precursor declines to a lower level, atoms tend to form nuclei and seeds through random hexagonal close packing, which contain stacking layer faults. In this case, the seeds usually have higher-energy structures and exhibit different shapes due to thermodynamic control.[14]

In this work, we use DMF as the solvent for the preparation of crystal seeds because this nonproton polar solvent is miscible with water. Besides, crystal seeds can grow directly in subsequent aqueous-based systems instead of undergoing

Received: March 25, 2024
Revised: May 24, 2024
Accepted: May 27, 2024
Published: June 14, 2024

purification steps (such as centrifugation) to obtain highly concentrated silver nanoplatelet crystals, which is favorable for industrial production on a large scale.

The prepared crystal seeds were prepared by the solvothermal method and then placed in an aqueous system for further growth. We successfully prepared silver nanoplates with different lateral dimensions (edge length: 565 nm−1.682 μm) and vertical sizes using a high-concentration silver source (217.3 mM). This synthesis route possesses benefits such as environmental friendliness, convenient operation, adjustable sizes, high product yield, and excellent repeatability. What is more, we provide a brand new strategy for the seed-mediated preparation of silver nanoplates.

2. EXPERIMENTAL SECTION

2.1. Reagents and Solvents. Silver nitrate ($AgNO_3$, >99%), *N*,*N*-dimethylformamide (DMF, >99.5%, Macklin), polyvinylpyrrolidone (PVP, MW = 40,000, Ourchem), cupric chloride dihydrate ($CuCl_2{\cdot}2H_2O$, 99.7%, Aladdin), deionized water are used in this study. All reagents and solvents were purchased from the suppliers and used without any purification.

2.2. Crystal Seed Solution Preparation. This Ag nanoplates were produced by the solvothermal method and then employed as the seeds for subsequent growth.[6,15−17] In a typical synthesis process, 12 g of PVP was first completely dissolved in 70 mL of DMF solution, and 0.37 g of $AgNO_3$ was then added to the mixture and stirred for 30 min at room temperature. The mixed solution was transferred to a three-necked flask and heated at 110 °C for 3 h under oil bath conditions. When the reaction was completed, the reactor was cooled to room temperature. Finally, the finished reaction solution is transferred to the glass bottle for use as crystal seed solution.

2.3. Synthesis of Silver Nanoplates with Different Lateral Dimensions. In a typical synthesis of triangular Ag nanoplates with an edge length of ∼1.682 μm, 3 g of PVP was added in 20 mL of H_2O at room temperature. Under magnetic stirring, 0.5 mL of crystal seed solution was added, and 20 mL of $AgNO_3$ (440 mM) was added in one portion subsequently. The mixed solution was thoroughly stirred and placed in an oven to initiate the growth of seeds. The reaction was processed at 85 °C for 72 h, followed by centrifugation to collect the triangular Ag nanoplates. To synthesize triangular Ag nanoplates of other lateral sizes, the volume of the seed solution was tuned.

Specifically, the volume of the seed solution was chosen to be 1.5 and 2.5 mL for the synthesis of triangular Ag nanoplates with average edge lengths of 778 and 565 nm, respectively.

2.4. Synthesis of Silver Nanoplates with Different Vertical Dimensions. In a typical synthesis of triangular Ag nanoplates with an edge length of ∼565 nm, 3 g of PVP was added in 20 mL of H_2O at room temperature. Under magnetic stirring, 0.5 mL of a crystal seed solution and 20 mL of $AgNO_3$ (440 mM) were added in one portion. The mixed solution was thoroughly stirred and placed in the oven to initiate the growth of seed. The reaction was allowed to proceed at 85 °C for 72 h. When the reaction was heated at 85 °C for 40 h, 0.5 mL of solution of $CuCl_2$ (0.2 M) was introduced into the system. Subsequently, the reaction solution was heated at 85 °C for 32 h until the reaction is finished. The preparation steps are shown schematically in Scheme 1.

Scheme 1. Schematic Diagram of the Experimental Preparation Steps

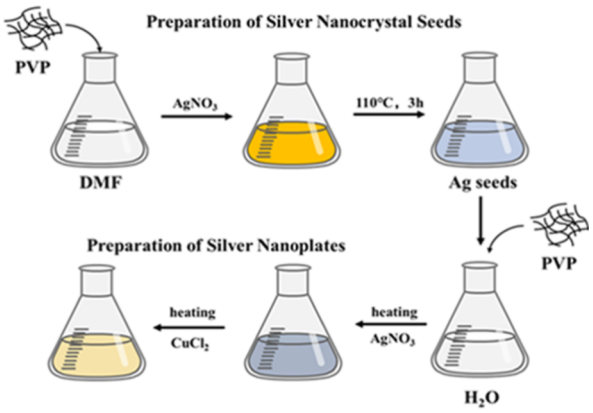

2.5. Characterizations. The size distribution of the synthesized crystal seeds was characterized by a UV−vis spectrophotometer (754PC, Shanghai Jinghua Technology Instrument Co., Ltd.). The synthesized silver nanoplates were characterized by X-ray diffraction (XRD MSAL-XD2). The morphological features of the samples were examined using scanning electron microscopy (SEM JSM-7610F) and transmission electron microscopy (TEM Talos F200X G2).

3. RESULTS AND DISCUSSION

3.1. Selection of Crystal Seeds. To get a macroanalysis of the size distribution and shape of the crystal seed solution, we employed a UV−vis spectrophotometer for its characterization. In order to find the crystal seed solution with a suitable size distribution, we followed the growth process of the crystal seeds, as shown in Figure 1.

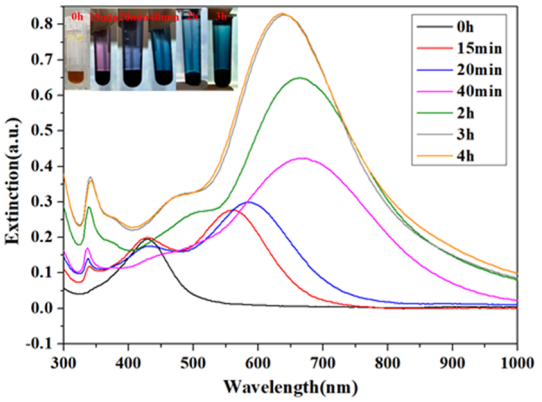

Figure 1. UV−vis absorption spectra of the seed solution aged at 110 °C for different times.

The characteristic peak position of the 0 h curve in Figure 1 appears near 425 nm, which corresponds to the out-of-plane dipole plasmon resonance of the silver nanoparticles and is consistent with the maximum absorption peak of the spherical silver particles. During this period, $AgNO_3$ reacted with DMF at ambient temperature to generate silver nanoparticles. Following heating at 110 °C for 15 min, the color of the solution changed from yellow to reddish-purple, as evidenced in Figure 1. Thereafter, two characteristic peaks were identified at 340 and 560 nm, respectively. These can be associated with the out-of-plane quadrupole plasmon resonance and in-plane

https://doi.org/10.1021/acsomega.4c02860
ACS Omega 2024, 9, 28659−28665

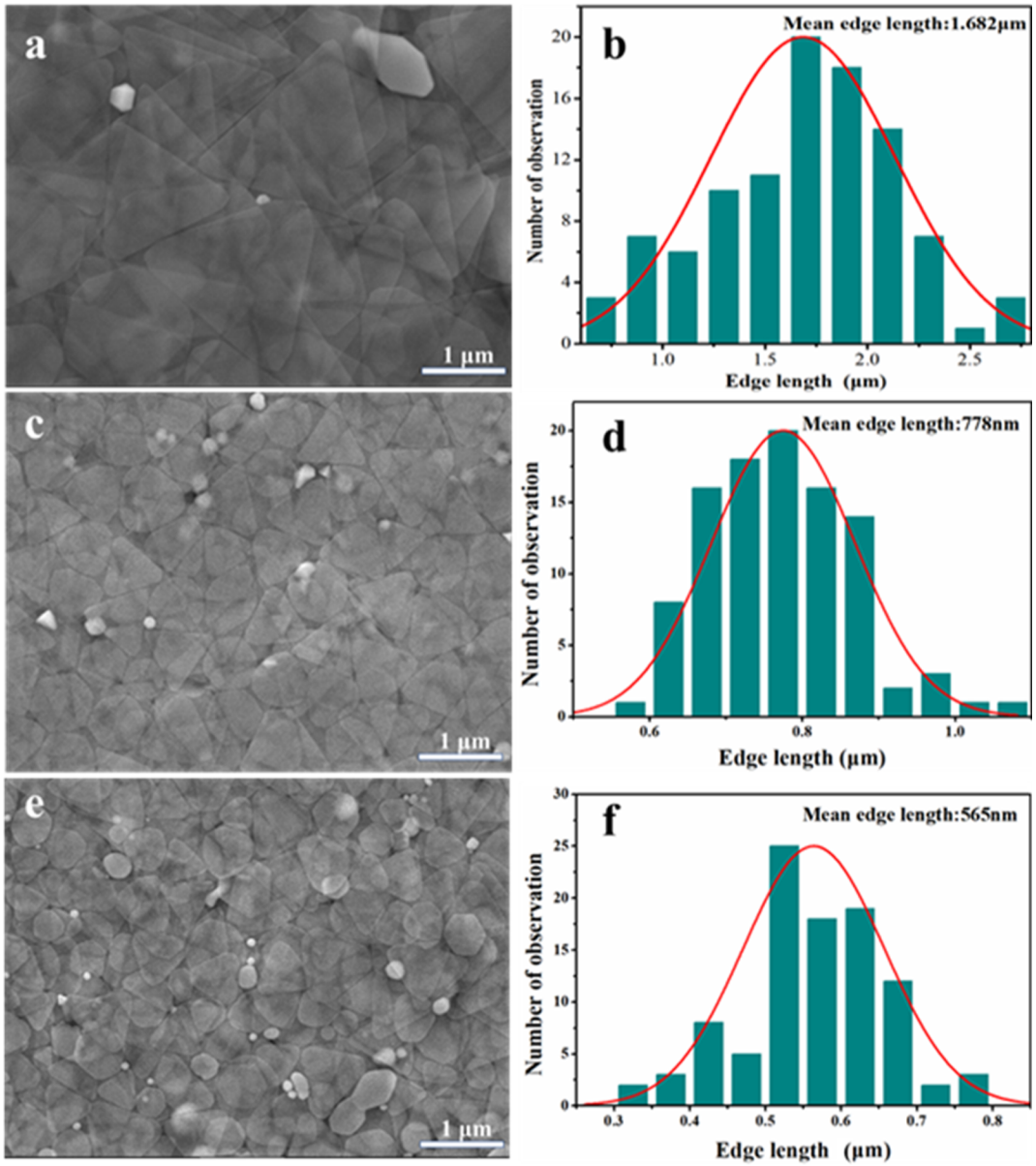

Figure 2. SEM images of the Ag nanoplates of different sizes obtained by tuning the volume of the seed solution. Seed volumes are (a) 0.5, (c) 1.5, and (e) 2.5 mL, respectively. (b,d,f) Are the particle size distribution curves corresponding to (a,c,e).

dipole plasmon resonance, respectively. The presence of these peaks confirms the generation of silver nanoplates in the solution. The characteristic peaks at 425 nm had a minimal alteration, which means the number of silver nanoparticles was almost unchanged. Thus, in the heating process, the continued generation of nanoparticles and the conversion of nanoparticles into nanoplates occurred simultaneously. During the following heating process (15 min−2 h), the characteristic peak at 425 nm gradually declines and disappears, leaving a certain degree of concave in the absorption curve. This indicates that the conversion of silver nanoparticles into silver nanoplates is the primary process at this stage. At this stage, we observed a redshift in the in-plane dipole plasmon resonance from 560 to 666 nm, indicating an increase in the lateral size of the silver nanoplates. This phenomenon confirms that the additional silver primarily originates from the reduction of the residual $AgNO_3$, and the edges of the nanoplate act as a heterogeneous nucleus for the deposition of Ag atoms. After heating for 3 h, the in-plane dipole plasmon resonance shows a slight blueshift from 666 to 638 nm. As shown in Figure 4a, a hexagonal silver nanoplate can be found in the crystalline seed solution and in consistent with the discrete dipole approximation simulations of Brioude et al.[18] It was deduced that the blueshift of the in-plane dipole resonance peaks is due to the transformation of the triangles into hexagons as a result of Oswald ripening.[18−20] When reaction solution was heated for 3 h, it could be seen that the UV−visible spectrum does not change at all, proving that the reaction has been completed. Therefore, we used the heating process of 110 °C for 3 h to prepare the crystal seed solution.

3.2. Control of the Lateral Size of Silver Nanoplates.

It was reported that PVP exhibits slightly weak reducing abilities and reacts slowly with Ag^+ at room temperature.[21] Thus, PVP functions as both a capping and reducing agent in this work, while $AgNO_3$ supplies Ag^+ as the Ag source. The growth process of seeds can be initiated by raising the reaction

https://doi.org/10.1021/acsomega.4c02860
ACS Omega 2024, 9, 28659−28665

Scheme 2. Schematic Diagram of the Nucleation Growth Mechanism of Crystal Seeds

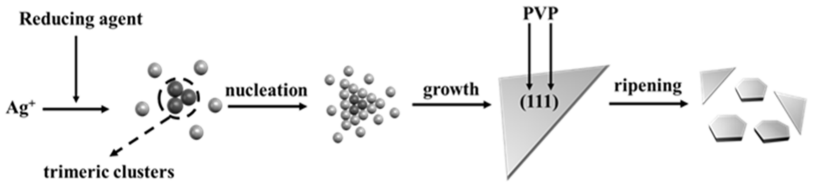

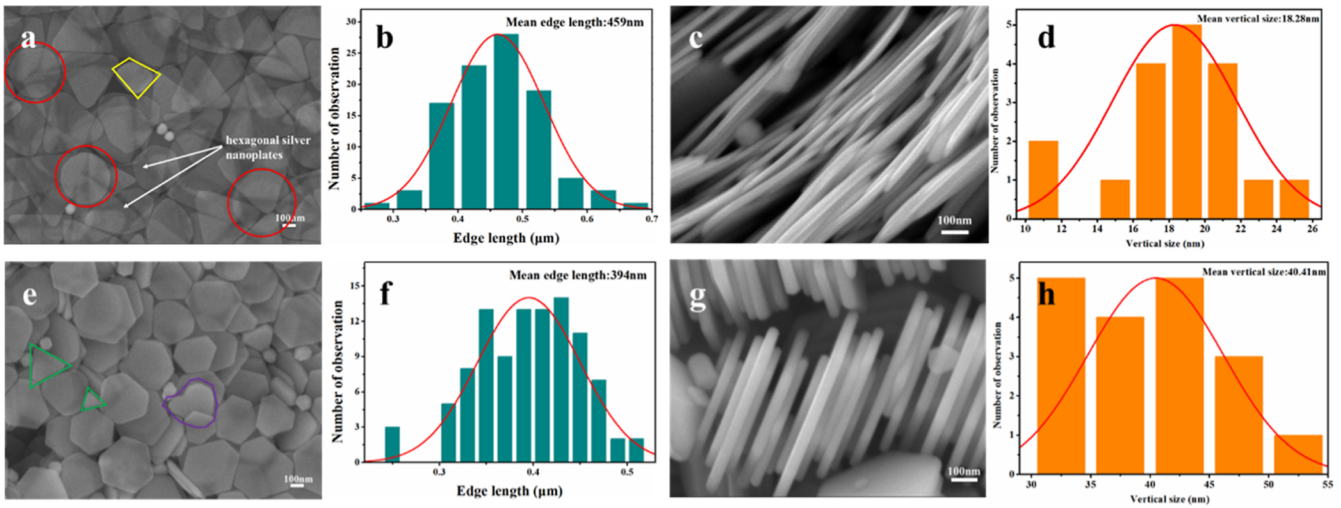

Figure 3. Effect of chloride ions on silver nanoplates: (a) SEM image of silver nanoplates synthesized without $CuCl_2$. (b) Lateral size distribution of silver nanoplates corresponding to (a). (c) SEM image of the thickness of silver nanoplates synthesized without $CuCl_2$. (d) Vertical size distribution of silver nanoplates corresponding to (c). (e) SEM image of silver nanoplates prepared in the presence of $CuCl_2$. (f) Lateral size distribution of silver nanoplates corresponding to (c). (g) SEM image of the thickness of silver nanoplates prepared in the presence of $CuCl_2$. (h) Vertical size distribution of silver nanoplates corresponding to (c).

temperature. Conversely, the reaction can be halted by swiftly lowering the temperature of the mixed solution. Furthermore, this synthesis method could tailor lateral size of the nanoplate by changing added volume of seed solution. Figure 2 shows the SEM images of silver nanoplates with different lateral dimensions after seed solution growth. In Figure 2, it can be seen that there is a high percentage of silver nanoplates and the particles are all regular platelike, which indicates that PVP as an end-capping agent can effectively guide the growth size of silver nanoplates. The synthesis process can prepare silver nanoplates in an aqueous solution with an Ag^+ concentration of 217.3 mM, which is less harmful to the environment and facilitates scale-up of the production as well.

The previous literature indicates that PVP exhibits a preference for binding to the Ag(100) crystal plane.[22] However, upon characterization of the silver nanoplates prepared by us through transmission methods depicted in Figure 4e,f, it became evident that the (111) crystalline surface of the silver nanoplates was binding to PVP instead of the (100) crystalline surface. Furthermore, it was revealed that the silver nanoplates experienced growth in the lateral direction. In this case, the researchers found that long-chain polymers can no longer effectively bind to the (100) crystal surface when the size drops below 15 nm.[23] In this synthesis, the silver nanoplates initiated growth on the crystal seeds. The size of the (100) crystal face of the seeds is less than 15 nm, while the size of the (111) crystal face is greater than 15 nm. Therefore, PVP can bind to only the (111) crystal face to achieve lateral growth. What is the role of PVP in the preparation of the silver nanoplates? It was deduced that PVP does not participate in surface coating during the transformation of silver nanoparticles to silver nanoplates in the initial stage of crystal seeds, meaning that when the size of the crystal surface of the triangle grows beyond 15 nm, it starts to combine with the crystal surface. We believe that the nucleation process of DMF-prepared crystal seeds is consistent with the findings of Xiong and coworkers.[24] During the early stages of the transformation process of silver nanoparticles, trimeric clusters of Ag_3^+ or Ag_3 are formed, which then reduce out of the silver atoms to act as a nucleus for growth. Eventually, triangular silver nanoplates are formed. This process is illustrated schematically in Scheme 2. This explains why PVP can be used to produce not only silver nanoplates but also other configurations such as silver nanorods or silver nanocubes.[25]

3.3. Control of the Vertical Size of Silver Nanoplate.

Silver nanoplate growth often involves both lateral and vertical dimensions, and a crystal plane may be terminated by end-capping agents to promote growth in the other direction. Halide ions, such as Cl^-, Br^-, and I^-, bind more strongly to the (100) crystal plane of silver than PVP. Therefore, introducing halide ions into the growth process allows for the control of lateral growth of silver nanoplates.[26]

In the presence of Cl^-, it tended to be absorbed by the faults and defect sites on the surface (100) preferentially, which reduced the surface energy of the faults dramatically, even lower than that on the surface (111). Therefore, growth in the direction of thickness is dominant. The lateral size of the silver nanoplates is 459 nm (Figure 3b), while their vertical size is 18.28 nm (Figure 3d). Following the introduction of a $CuCl_2$ solution into the system, the lateral size of the nanoplates

https://doi.org/10.1021/acsomega.4c02860
ACS Omega 2024, 9, 28659−28665

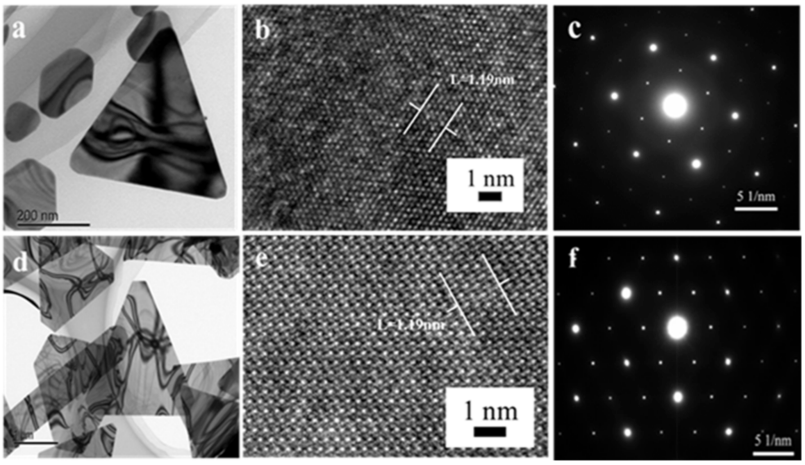

Figure 4. TEM characterizes seeds and silver nanoplates. (a−c) Correspond to the TEM images of the crystal seeds, lattice fringe, and selective electron diffraction, respectively. (d−f) Correspond to TEM images of the nanoplates with a transverse size of 1.682 μm, lattice fringes, and selective electron diffraction.

decreased to 394 nm (Figure 3d), while their vertical size increased to 40.41 nm. Additionally, before the addition of $CuCl_2$, the shapes of the silver nanoplates were mainly triangular. After the addition of $CuCl_2$, the nanoplates were mainly transf to hexagonal nanoplates with very few triangular nanoplates.[27] However, there are only two truncated triangular silver nanoplates observed in Figure 3e, but in theory, there should be three times as many truncated triangles as hexagonal silver nanoplates. A preliminary guess is that the sharp corner of the truncated silver triangle may dissolve into small clusters due to high surface energy combined with the heat energy brought by the heating process in the oven and then grow to the (111) crystal plane of the silver slice through nonclassical growth.[28]

3.4. Characterization of Seeds and Silver Nanoplates.

Figure 4 shows TEM images of a typical sample. As shown in Figure 4a, the seed solution contained triangular silver nanoplates and hexagonal silver nanoplates. After growth, the silver nanoplates are mainly triangular. Some studies suggest that the shape transformation of face-centered cubic metal is caused by the change of reduction rate,[21,29] and increasing the reduction rate appropriately is conducive to the transformation of hexagonal nanoplates to triangular nanoplates. As shown in Figure 4b,e, the lattice fringe of the seed and triangular silver nanoplate exhibits a typical face-centered cubic hexagonal symmetry and a neat arrangement of atoms. Five lattice fringes are selected to measure the spacing of 1.19 nm, and it can be seen that the lattice spacing of 0.238 nm is the same as that of the silver (111) plane.[30] It proved that the seeds maintained a good atomic arrangement after subsequent growth. Figure 4c shows a clear hexagonal lattice diffraction pattern, which is determined by the cell structure of the single-crystal silver plate and verifies that the silver grown in this experiment is a single crystal.

The samples were qualitatively characterized by the XRD test. Silver nanosheet solution was prepared into powder and characterized by XRD, which is shown in Figure 5. The positions of the XRD peaks of the triangular Ag nanoparticle are 38, 44, 64, and 77° respectively, corresponding to the crystal faces of (111), (200), (220), and (311), respectively (JCPDS no. 04-0783), which proves that the prepared silver nanoplates have high purity and no impurities such as silver oxides.

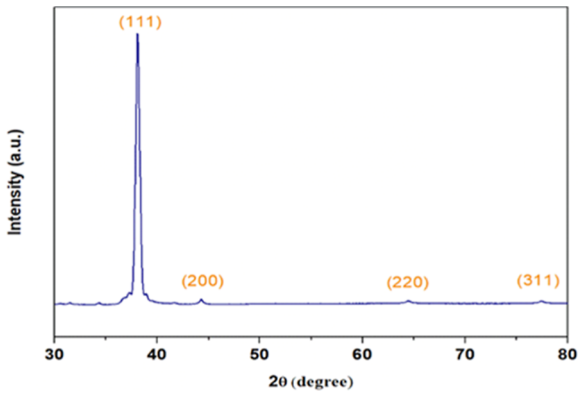

Figure 5. XRD of silver nanoplates after seed growth.

Additionally, this synthesis can be readily scaled up to produce a large quantity of Ag nanoplates due to the weak reduction and good coating effect of PVP effectively inhibiting the self-nucleation behavior of silver atoms after reduction. We carried out a scale-up experiment. After the experiment was enlarged 10 times, 9.3 g of silver nanoplates with a lateral size of 1.582 μm were obtained, and yield can reach 97%.

Figure 6 shows the digital and SEM images of a silver nanoplate sol obtained after the scale-up experiment. As we can see, the shapes are basically triangular and almost identical to those obtained from typical scale synthesis (Figure 2a), and the sizes of the triangular silver nanoplates are close to the target size. Thus, our scale-up synthesis experiment achieves the desired effect. Besides, the synthesis method can prepare silver nanoplates in batches and has high practical value.

4. CONCLUSION

In summary, we synthesized silver nanoplates with lateral sizes ranging from 565 nm to 1.682 μm at an Ag^+ concentration of 217.3 mM by means of seed growth and attempted to achieve anisotropic growth of silver nanoplates with longitudinal thickness control. This method uses the weak reduction ability of PVP to inhibit self-nucleation. Anisotropic growth of silver nanoplates was achieved by PVP and chloride ions. This synthesis method is simple and easy to operate, environmental friendly, and can achieve one-step mass production while ensuring product quality. This work provides a new idea for

https://doi.org/10.1021/acsomega.4c02860
ACS Omega 2024, 9, 28659−28665

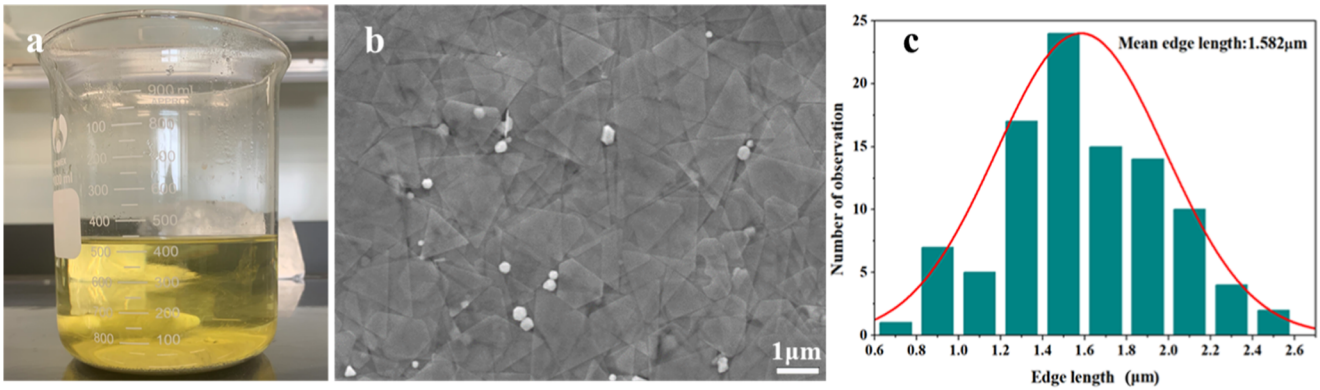

Figure 6. Large-scale synthesis of triangular Ag nanoplates. Target edge length: 1.582 μm; practical weight of product: 9.3 g. (a) Digital photograph of the sol of the Ag nanoplates after silver nanoplates settle to the bottom of the beaker. (b) Typical SEM image. (c) Size distribution of the Ag nanoplates measured by SEM imaging.

the batch preparation of silver nanoplates: the crystalline seeds are prepared by solvothermal method and then placed in an aqueous system to regulate the size of silver nanoplates.

■ ASSOCIATED CONTENT

Supporting Information

The Supporting Information is available free of charge at https://pubs.acs.org/doi/10.1021/acsomega.4c02860.

Comparison of silver nanoplate preparation methods, main components being precursor, solvent, end-capping agent, reducing agent, and Ag^+ concentration (PDF)

■ AUTHOR INFORMATION

Corresponding Authors

Yanhong Zhao − *State Key Laboratory of Advanced Materials for Smart Sensing, GRINM Group Co., Ltd., Beijing 100088, China; GRIMAT Engineering Institute Co., Ltd., Beijing 101407, China; General Research Institute for Nonferrous Metals, Beijing 100088, China;* orcid.org/0009-0007-0244-6988; Email: zhaoyanhong@grinm.com

Zhimin Yang − *State Key Laboratory of Advanced Materials for Smart Sensing, GRINM Group Co., Ltd., Beijing 100088, China; GRIMAT Engineering Institute Co., Ltd., Beijing 101407, China; General Research Institute for Nonferrous Metals, Beijing 100088, China*; Email: power@grinm.com

Authors

Zhenbin Zhang − *State Key Laboratory of Advanced Materials for Smart Sensing, GRINM Group Co., Ltd., Beijing 100088, China; Institute for Advanced Materials and Technology, University of Science and Technology Beijing, Beijing 100083, China; GRIMAT Engineering Institute Co., Ltd., Beijing 101407, China; General Research Institute for Nonferrous Metals, Beijing 100088, China*

Tanlong Xue − *State Key Laboratory of Advanced Materials for Smart Sensing, GRINM Group Co., Ltd., Beijing 100088, China; GRIMAT Engineering Institute Co., Ltd., Beijing 101407, China; General Research Institute for Nonferrous Metals, Beijing 100088, China*

Mingli Qin − *Institute for Advanced Materials and Technology, University of Science and Technology Beijing, Beijing 100083, China;* orcid.org/0000-0002-4001-6539

Yanzhao Wang − *State Key Laboratory of Advanced Materials for Smart Sensing, GRINM Group Co., Ltd., Beijing 100088, China; GRIMAT Engineering Institute Co., Ltd., Beijing 101407, China; General Research Institute for Nonferrous Metals, Beijing 100088, China*

Qi Shi − *State Key Laboratory of Advanced Materials for Smart Sensing, GRINM Group Co., Ltd., Beijing 100088, China; GRIMAT Engineering Institute Co., Ltd., Beijing 101407, China; General Research Institute for Nonferrous Metals, Beijing 100088, China*

Lulu Wang − *State Key Laboratory of Advanced Materials for Smart Sensing, GRINM Group Co., Ltd., Beijing 100088, China; GRIMAT Engineering Institute Co., Ltd., Beijing 101407, China; General Research Institute for Nonferrous Metals, Beijing 100088, China*

Complete contact information is available at: https://pubs.acs.org/10.1021/acsomega.4c02860

Notes

The authors declare no competing financial interest.

■ ACKNOWLEDGMENTS

This publication is the result of research funded under the Low-Temperature Pressureless Sintering of High-Thermal Conductivity Silver Paste project, a research grant funded by the Innovation Fund of the Arigatou Research Institute of Engineering and Technology (grant no. 5272215).

■ REFERENCES

(1) Kumar Chandraker, S.; Lal, M.; Kumar Ghosh, M.; Ram, T.; Paliwal, R.; Shukla, R. Biofabrication of spherical silver nanoparticles using leaf extract of Plectranthus barbatus Andrews: characterization, free radical scavenging, and optical properties. *Inorg. Chem. Commun.* **2022**, *142*, 109669.

(2) Zhang, Z.; Fu, G.; Wan, B.; Su, Y.; Jiang, M. Research on sintering process and thermal conductivity of hybrid nanosilver solder paste based on molecular dynamics simulation. *Microelectron. Reliab.* **2021**, *126*, 114203.

(3) Kaiser, K. G.; Delattre, V.; Frost, V. J.; Buck, G. W.; Phu, J. V.; Fernandez, T. G.; Pavel, I. E. Nanosilver: An Old Antibacterial Agent with Great Promise in the Fight against Antibiotic Resistance. *J. Antibiot.* **2023**, *12* (8), 1264.

(4) Haynes, C. L.; Mcfarland, A. D.; Zhao, L.; Van Duyne, R. P.; Schatz, G. C.; Gunnarsson, L.; Prikulis, J.; Kasemo, B.; Käll, M. Nanoparticle optics: the importance of radiative dipole coupling in two-dimensional nanoparticle arrays. *J. Phys. Chem. B* **2003**, *107* (30), 7337−7342.

(5) Pastoriza-Santos, I.; Liz-Marzán, L. M. Colloidal silver nanoplates. State of the art and future challenges. *J. Mater. Chem.* **2008**, *18* (15), 1724−1734.
(6) Wang, C.; Li, G.; Xu, L.; Li, J.; Zhang, D.; Zhao, T.; Sun, R.; Zhu, P. Low Temperature Sintered Silver Nanoflake Paste for Power Device Packaging and Its Anisotropic Sintering Mechanism. *ACS Appl. Electron. Mater.* **2021**, *3* (12), 5365−5373.
(7) Peng, Y.; Raj, N.; Strasser, J. W.; Crooks, R. M. Paper Biosensor for the Detection of NT-proBNP Using Silver Nanodisks as Electrochemical Labels. *Nanomaterials* **2022**, *12* (13), 2254.
(8) Han, Y. D.; Zhang, S. M.; Jing, H. Y.; Wei, J.; Bu, F. H.; Zhao, L.; Lv, X. Q.; Xu, L. Y. The fabrication of highly conductive and flexible Ag patterning through baking Ag nanosphere−nanoplate hybrid ink at a low temperature of 100 °C. *Nanotechnology* **2018**, *29* (13), 135301.
(9) Jin, R.; Cao, Y.; Mirkin, C. A.; Kelly, K. L.; Schatz, G. C.; Zheng, J. G. Photoinduced conversion of silver nanospheres to nanoprisms. *Science* **2001**, *294* (5548), 1901−1903.
(10) Zhang, Q.; Hu, Y.; Guo, S.; Goebl, J.; Yin, Y. Seeded Growth of Uniform Ag Nanoplates with High Aspect Ratio and Widely Tunable Surface Plasmon Bands. *Nano Lett.* **2010**, *10* (12), 5037−5042.
(11) Liu, X.; Li, L.; Yang, Y.; Yin, Y.; Gao, C. One-step growth of triangular silver nanoplates with predictable sizes on a large scale. *Nanoscale* **2014**, *6* (9), 4513−4516.
(12) Zeng, J.; Xia, X.; Rycenga, M.; Henneghan, P.; Li, Q.; Xia, Y. Successive Deposition of Silver on Silver Nanoplates: Lateral versus Vertical Growth. *Angew. Chem., Int. Ed.* **2011**, *50* (1), 244−249.
(13) Xia, Y.; Xia, X.; Peng, H. C. Shape-Controlled Synthesis of Colloidal Metal Nanocrystals: Thermodynamic versus Kinetic Products. *J. Am. Chem. Soc.* **2015**, *137* (25), 7947−7966.
(14) Xiong, Y.; Siekkinen, A. R.; Wang, J.; Yin, Y.; Kim, M. J.; Xia, Y. Synthesis of silver nanoplates at high yields by slowing down the polyol reduction of silver nitrate with polyacrylamide. *J. Mater. Chem.* **2007**, *17* (25), 2600−2602.
(15) Zhang, Z.; Yu, J.; Zhang, J.; Lian, Y.; Shi, Z.; Cheng, Z.; Gu, M. pH-controlled growth of triangular silver nanoprisms on a large scale. *Nanoscale Adv.* **2019**, *1* (12), 4904−4908.
(16) Pastoriza-Santos, I.; Liz-Marzán, L. M. Colloidal silver nanoplates. State of the art and future challenges. *J. Mater. Chem.* **2008**, *18* (15), 1724−1734.
(17) Lai, Y.-C.; Wang, Y.-C.; Chiu, Y.-C.; Liao, Y.-C. Microwave-Assisted Synthesis for Silver Nanoplates with a High Aspect Ratio. *Langmuir* **2021**, *37* (46), 13689−13695.
(18) Brioude, A.; Pileni, M. P. Silver Nanodisks: Optical Properties Study Using the Discrete Dipole Approximation Method. *J. Phys. Chem. B* **2005**, *109* (49), 23371−23377.
(19) Chen, X.; Liu, X.; Huang, K. Synthesis of uniform hexagonal Ag nanoprisms with controlled thickness and tunable surface plasmon bands. *Int. J. Miner., Metall. Mater.* **2019**, *26* (6), 796−802.
(20) Liu, M.; Leng, M.; Yu, C.; Wang, X.; Wang, C. Selective synthesis of hexagonal Ag nanoplates in a solution-phase chemical reduction process. *Nano Res.* **2010**, *3* (12), 843−851.
(21) Xiong, Y.; Washio, I.; Chen, J.; Cai, H.; Li, Z.-Y.; Xia, Y. Poly(vinyl pyrrolidone): a dual functional reductant and stabilizer for the facile synthesis of noble metal nanoplates in aqueous solutions. *Langmuir* **2006**, *22* (20), 8563−8570.
(22) AL-Saidi, W. A.; Feng, H.; Fichthorn, K. A. Adsorption of polyvinylpyrrolidone on Ag surfaces: insight into a structure-directing agent. *Nano Lett.* **2012**, *12* (2), 997−1001.
(23) Ruditskiy, A.; Xia, Y. Toward the Synthesis of Sub-15 nm Ag Nanocubes with Sharp Corners and Edges: The Roles of Heterogeneous Nucleation and Surface Capping. *J. Am. Chem. Soc.* **2016**, *138* (9), 3161−3167.
(24) Xiong, Y.; Washio, I.; Chen, J.; Sadilek, M.; Xia, Y. Trimeric Clusters of Silver in Aqueous $AgNO_3$ Solutions and Their Role as Nuclei in Forming Triangular Nanoplates of Silver. *Angew. Chem., Int. Ed.* **2007**, *46* (26), 4917−4921.
(25) Zhu, Z.; Wang, X.; Yu, H.; Zhou, W.; Wang, Y.; Han, J.; Guo, F. Improved Polyol Syntheses of Silver Right Bipyramids and Nanorods: Camphorquinone-Mediated Morphology Control Methods. *Cryst. Growth Des.* **2023**, *23* (3), 1455−1465.
(26) Yang, T. H.; Shi, Y.; Janssen, A.; Xia, Y. Surface Capping Agents and Their Roles in Shape-Controlled Synthesis of Colloidal Metal Nanocrystals. *Angew. Chem., Int. Ed.* **2020**, *59* (36), 15378−15401.
(27) Tan, T.; Yao, L.; Liu, H.; Li, C.; Wang, C. Precise Control of the Lateral and Vertical Growth of Two-Dimensional Ag Nanoplates. *Chem.—Eur. J.* **2017**, *23* (42), 10001−10006.
(28) Jun, Y.-S.; Zhu, Y.; Wang, Y.; Ghim, D.; Wu, X.; Kim, D.; Jung, H. Classical and Nonclassical Nucleation and Growth Mechanisms for Nanoparticle Formation. *Annu. Rev. Phys. Chem.* **2022**, *73*, 453−477.
(29) Xiong, Y.; Mclellan, J. M.; Chen, J.; Yin, Y.; Li, Z.-Y.; Xia, Y. Kinetically controlled synthesis of triangular and hexagonal nanoplates of palladium and their SPR/SERS properties. *J. Am. Chem. Soc.* **2005**, *127* (48), 17118−17127.
(30) Xiong, Y.; Xie, Y.; Wu, C.; Yang, J.; Li, Z.; Xu, F. Formation of silver nanowires through a sandwiched reduction process. *Adv. Mater.* **2003**, *15* (5), 405−408.

https://doi.org/10.1021/acsomega.4c02860
ACS Omega 2024, 9, 28659−28665